Department of Applied Physics

Atomic and electronic transport on surfaces and interfaces

Mikko Hakala

Aalto University

DOCTORAL DISSERTATIONS

Aalto University publication series
DOCTORAL DISSERTATIONS 219/2013

Atomic and electronic transport on surfaces and interfaces

Mikko Hakala

A doctoral dissertation completed for the degree of Doctor of Science in Technology to be defended, with the permission of the Aalto University School of Science, at a public examination held at the lecture hall C of the Aalto University on 24th of January 2014 at 13 o'clock.

Aalto University
School of Science
Department of Applied Physics
COMP/SIN

Supervising professors
Distinguished Prof. Risto Nieminen
Prof. Adam Foster

Preliminary examiners
Prof. Matti Alatalo, Lappeenranta University of Technology, Finland
Prof. Esa Räsänen, Tampere University of Technology, Finland

Opponent
Prof. Keith McKenna, University of York, UK

Aalto University publication series
DOCTORAL DISSERTATIONS 219/2013

ISBN 978-952-60-5513-8
ISBN 978-952-60-5514-5 (pdf)
ISSN-L 1799-4934
ISSN 1799-4934 (printed)
ISSN 1799-4942 (pdf)
http://urn.fi/URN:ISBN:978-952-60-5514-5

Unigrafia Oy
Helsinki 2013

Finland

Aalto University

Abstract

Aalto University, P.O. Box 11000, FI-00076 Aalto www.aalto.fi

Author
Mikko Hakala

Name of the doctoral dissertation
Atomic and electronic transport on surfaces and interfaces

Publisher School of Science

Unit Department of Applied Physics

Series Aalto University publication series DOCTORAL DISSERTATIONS 219/2013

Field of research Computational Physics

Manuscript submitted 20 August 2013 **Date of the defence** 24 January 2014

Permission to publish granted (date) 10 September 2013 **Language** English

☐ **Monograph** ☒ **Article dissertation (summary + original articles)**

Abstract

The properties of interfaces and surfaces play a key role in the functional design of many technologies, particularly in the development of next generation micro-electronic devices and nanocatalysts. In micro-electronics, hafnia is seen as a reliable replacement for silica in modern transistors, yet little is known about its interface with silicon and probable defects formed. Similarly, the formation of metallic nanoparticles on insulators is a promising route to new catalytically active materials, but much work is needed to understand the dynamical growth of these particles on surfaces from deposited metal atoms.

In this thesis we have modeled the properties of defects in silicon-hafnia interfaces and metal adatoms on alkali halide surfaces. The calculations have been performed within the density-functional theory (DFT), supported by electron transport calculations for the interface studies. Although these results have been successful in building our understanding, we have identified the need to enhance the accuracy of the standard DFT approach without sacrificing computational speed. For this we have implemented efficient hybrid functionals into the SIESTA code and shown that it indeed improves our description of critical materials' properties.

Keywords density-functional theory, interfaces, surfaces, exchange

ISBN (printed) 978-952-60-5513-8 **ISBN (pdf)** 978-952-60-5514-5

ISSN-L 1799-4934 **ISSN (printed)** 1799-4934 **ISSN (pdf)** 1799-4942

Location of publisher Helsinki **Location of printing** Helsinki **Year** 2013

Pages 114 **urn** http://urn.fi/URN:ISBN:978-952-60-5514-5

Aalto-yliopisto

Tiivistelmä

Aalto-yliopisto, PL 11000, 00076 Aalto www.aalto.fi

Tekijä
Mikko Hakala

Väitöskirjan nimi
Elektronien kuljetus pinnoilla ja rajapinnoilla

Julkaisija Perustieteiden korkeakoulu

Yksikkö Teknillisen fysiikan laitos

Sarja Aalto University publication series DOCTORAL DISSERTATIONS 219/2013

Tutkimusala Laskennallinen fysiikka

Käsikirjoituksen pvm 20.08.2013 **Väitöspäivä** 24.01.2014

Julkaisuluvan myöntämispäivä 10.09.2013 **Kieli** Englanti

☐ **Monografia** ☒ **Yhdistelmäväitöskirja (yhteenveto-osa + erillisartikkelit)**

Tiivistelmä

Pintojen ja rajapintojen ominaisuudet ovat merkittävässä roolissa kehitettäessä useita teknologioita. Mikroelektronisten laitteiden kohdalla hafniumoksidi nähdään luotettavana vaihtoehtona korvaamaan piioksidi seuraavan sukupolven transistoreissa. Kuitenkin sen rakenteesta ja virheiden muodostumisesta piin rajapinnassa tiedetään varsin vähän. Vastaavasti nanokatalyysin kohdalla metalliset nanopartikkelit eristepinnoilla tarjoavat lupaavan polun luoda uusia katalyyttisesti aktiivisia materiaaleja. Mutta paljon työtä vaaditaan, jotta ymmärretään näiden partikkelien muodostumista ja kasvua pinnoille tuoduista metalliatomeista.

Tässä väitöskirjassa on mallinnettu virheiden ominaisuuksia pii--hafiumoksidi-rajapinnoilla ja metallisten atomien diffuusiota alkalihalidipinnoilla. Laskut on suoritettu käyttäen tiheysfunktionaaliteoriaa (DFT). Lisäksi rajapintojen kohdalla on tutkimusta täydennetty mallintamalla elektronien kuljetusta. Tulokset ovat antaneet erinomaista tietoa tutkituista ominaisuuksista, mutta samalla näille rakenteille olemme havainneet, että tiheysfunktionaaliteoriassa käytettävien kunktionaalien tarkkuutta tulee parantaa. Tätä varten olemme implementoineet tehokkaan hybridifunktionaalimenetelmän SIESTA koodiin ja osoittaneet, että tämä todella parantaa laskennallista kuvaa materiaalien ominaisuuksista.

Avainsanat tiheysfunktionaaliteoria, pinnat, rajapinnat

ISBN (painettu) 978-952-60-5513-8 **ISBN (pdf)** 978-952-60-5514-5

ISSN-L 1799-4934 **ISSN (painettu)** 1799-4934 **ISSN (pdf)** 1799-4942

Julkaisupaikka Helsinki **Painopaikka** Helsinki **Vuosi** 2013

Sivumäärä 114 **urn** http://urn.fi/URN:ISBN:978-952-60-5514-5

Preface

This thesis has been prepared in the Computational Nanoscience group (COMP) in the Department of Applied Physics, Aalto University, during 2005-2013. I thank Acad. Prof Risto Nieminen for the opportunity to work in the COMP group and for the supervision.

I wish to express my gratitude to Prof. Adam Foster for his supervision. He has been guiding me patiently and allowed me to follow my own path in doing science and created an excellent atmosphere for scientific discussions.

I would also like to acknowledge my collaborations and colleagues at Aalto (TKK) and Curtin University of Technology, Perth, for advice, ideas, practical help and good times they have provided. I am especially grateful to Andris Gulans whose aid and ideas were remarkable.

I have been personally supported by a grant from the CSC, the Finnish IT Center for science administered by the Ministry of Education. CSC has also provided the main part of the computational resources for this work. This support is gratefully acknowledged.

Espoo,

Mikko Hakala

Contents

List of publications

This thesis consists of an overview and the following publications:

I Hakala, M. H., Foster, A. S., Gavartin, J.L., Havu, P., Puska, M. J. and Nieminen R. M. *Interfacial oxide growth at silicon/high-k oxide interfaces: First principles modeling of the Si-HfO_2 interface*, Journal of Applied Physics 100, 043708 (2006)

II Havu, P., Havu V., Puska, M. J., Hakala, M. H., Foster, A. S. and Nieminen R. M. *Finite-element implementation for electron transport in nanostructures*, Journal of Chemical Physics 124, 054707 (2006)

III Hakala, M. H., Pakarinen, O. H. and Foster, A. S., *First principles study of adsorption, diffusion and charge stability of metal adatoms on alkali halide surfaces*, Physical Review B 78, 045418 (2008)

IV Hakala, M. H. and Foster, A. S. *Computationally efficient implementation of hybrid functionals in SIESTA*, Aalto University publication series SCIENCE + TECHNOLOGY, 19 (2013)

The author has had an active role in all the phases of the research reported in this thesis. He has developed the computer code used in Publication IV and algorithms used in Publication III. The author has performed structure and electronic properties calculations in Publication I and II, all the calculation in the Publication III and IV, and has constructed the structure used in calculations in Publication III. He has written the first draft of Publication I, III and IV.

1. Introduction

This thesis has been divided into two parts. In the first half we have studied a few of the key properties and processes that define the properties of interfaces and surfaces. For interfaces in general, the defects can seriously affect or even determine the macroscopic properties of materials even though their size is only of order of few atoms and the concentration a few ppm. They affect diffusion, and especially in semiconducting materials, they are electronically active. They can reduce channel mobility, increase leakage current and change the optical properties of the material.

For surfaces the adatom absorption and diffusion is an important step in predicting the growth properties of deposited material. Especially on insulating crystal and thin film surfaces the absorption of metal adatoms forming nanoclusters is important in understanding the catalytic properties of these nanoclusters. For these systems the charge transfer between the surface and the absorbed metal atom also influences the reactivity of the nanocluster.

Computational methods mentioned in this thesis, namely density functional theory, have been applied to study the properties $Si - HfO_2$ interfaces and metal adatoms on alkali halide surfaces. By creating an atomic scale model and starting from first principles we obtain detailed information of the system. These results can then be used to help the design of better devices and provide explanation of experimental results.

Although widely used and found successful, we find that the methods we have used in the first part of thesis do not provide high enough accuracy in all aspects. To make reliable predictions in the previous cases we need to describe defect levels and charge localization with higher accuracy. The second part of the thesis focuses on implementing a better

method as implemented in so-called the hybrid functionals, and showing that we indeed improve our description of materials properties.

Our implementation is validated by calculating the properties of five materials with different electronic properties. The predictive power of the hybrid method is compared against the results of standard PBE-functional and different implementations of hybrid functional approach are considered.

The results of this work have been published in articles I-IV. In publication I a model $Si - HfO_2$ interface is grown and the properties of defect states are studied. Publication II explains Green's functions transport method and applies this to the same silicon hafnia interface to obtain information applicable to real life leakage current. Article III concentrates on absorption, diffusion and charge stability of metal adatoms of gold, silver and palladium on the surfaces of NaCl, KCl and KBr.

In article IV we present our implementation of the hybrid functionals into the Siesta density functional code and validate the approach by studying five materials with different electronic properties. The implementation of hybrid functional into the SIESTA code has been the most demanding part of this thesis and in addition to the result, this thesis focuses on describing the used approach thoroughly.

2. Theory and models

The physics of studied systems at the atomic scale often need to be described by quantum mechanics. The properties of a quantum mechanical many-body system are calculated from the many-particle Schrödinger equation

$$\hat{\mathbf{H}}\Psi(\mathbf{r}_1,\ldots,\mathbf{r}_N) = E\Psi(\mathbf{r}_1,\ldots,\mathbf{r}_N), \tag{2.1}$$

where E is the energy of the many-particle electron state. The Hamiltonian of a system of N interacting electrons at sites $\mathbf{r}_i$ and nuclei with charge $\mathbf{Z}_i$ and masses $\mathbf{M}_I$ at sites $\mathbf{R}_I$ is given by

$$\begin{aligned} H(\mathbf{r}) \quad &= -\tfrac{1}{2}\sum_i \nabla_i^2 - \sum_{i,I}\frac{Z_I}{|\mathbf{r}_i-\mathbf{R}_I|} + \frac{1}{2}\sum_{i\neq j}\frac{1}{|\mathbf{r}_i-\mathbf{r}_j|} \\ &\quad - \sum_I \frac{1}{2M_I}\nabla_I^2 + \frac{1}{2}\sum_{I\neq J}\frac{1}{|\mathbf{R}_I-\mathbf{R}_J|}. \end{aligned} \tag{2.2}$$

All units are given in atomic units. As the inverse masses of nuclei are very small it is common to first assume the kinetic energy of atoms to be zero while solving the equation for electronic degrees of freedom. Then later the nuclei degrees of freedom are treated classically. This is the so-called Born-Oppenheimer or adiabatic approximation.

While methods for solving this equation directly exist, they are computationally extremely expensive and thus only applicable to systems with a small number of electrons.

In the framework of this thesis, two approaches to solve the adiabatic approximation of the quantum many-body problem are applied: Density functional theory (DFT) and a hybrid method combining DFT and Hartree-Fock (HF) method calculated with Kohn-Sham orbitals. Both HF and DFT are approximative methods and, in principle, provide information only on the ground state of the system.

2.1 Hartree-Fock theory

In Hartree-Fock theory[1] the many-body picture is simplified by assuming all electrons to be uncorrelated except via the antisymmetricity of the fermionic wavefunction. This mentioned correlation of electrons of the same spin is called the *exchange* and all the other electron correlation is usually referred simply as *correlation*. This terminology is also adopted in this thesis. The correlation term in the Hartree-Fock theory is assumed to be zero.

With these assumptions one can now write the electronic wavefunction as a determinant of single particle wavefunctions

$$\Psi_{AS}(\mathbf{r}_1,\ldots,\mathbf{r}_N) = \begin{vmatrix} \Psi_1(\mathbf{r}_1) & \Psi_2(\mathbf{r}_1) & \ldots & \Psi_N(\mathbf{r}_1) \\ \Psi_1(\mathbf{r}_2) & \Psi_2(\mathbf{r}_2) & \ldots & \Psi_N(\mathbf{r}_2) \\ \vdots & \vdots & & \vdots \\ \Psi_1(\mathbf{r}_N) & \Psi_2(\mathbf{r}_N) & \ldots & \Psi_N(\mathbf{r}_N) \end{vmatrix}. \tag{2.3}$$

If one now writes the many-body Hamiltonian as

$$\begin{aligned} H &= \sum_i h(i) + \frac{1}{2}\sum_{i,j;i\neq j} g(i,j) \\ g(i,j) &= \frac{1}{|\mathbf{r}_i - \mathbf{r}_j|} \\ h(i) &= -\frac{1}{2}\nabla_i^2 - \sum_n \frac{Z_n}{|\mathbf{r}_i - \mathbf{R}_n|}, \end{aligned} \tag{2.4}$$

then the expectation value of the energy becomes into a form of

$$\begin{aligned} E_{HF} &= \langle \Psi_{AS}|H|\Psi_{AS}\rangle \\ &= \sum_i \langle \Psi_i|h|\Psi_i\rangle \\ &+ \frac{1}{2}\sum_{ij}[\langle \Psi_k\Psi_l|\Psi_k\Psi_l\rangle - \langle \Psi_k\Psi_l|\Psi_l\Psi_k\rangle] \\ \langle \Psi_k\Psi_l|\Psi_m\Psi_n\rangle &= \int dr_1 dr_2 \Psi_k^*(\mathbf{r}_1)\Psi_l^*(\mathbf{r}_2)\frac{1}{|\mathbf{r}_i - \mathbf{r}_j|}\Psi_m(\mathbf{r}_1)\Psi_n(\mathbf{r}_2) \end{aligned} \tag{2.5}$$

For the two electron integrals we can simplify equation 2.5 by defining operators

$$\begin{aligned} J(\mathbf{r})\Psi(\mathbf{r}) &= \sum_k \int dr' \Psi_k^*(\mathbf{r}')\frac{1}{r_{12}}\Psi_k(\mathbf{r}')\Psi(\mathbf{r}) \\ K(\mathbf{r})\Psi(\mathbf{r}) &= \sum_k \int dr' \Psi_k^*(\mathbf{r}')\frac{1}{r_{12}}\Psi(\mathbf{r}')\Psi_k(\mathbf{r}), \end{aligned} \tag{2.6}$$

where J is called the Coulombic operator and K the exchange operator. With these operators we can write the total energy as

$$E = \sum_k \left\langle \Psi_k | h + \frac{1}{2}(J - K) | \Psi_k \right\rangle . \tag{2.7}$$

In practical calculations this equation would be then written into matrix form using proper basis functions. And the energy and solution to the ground state is obtained with minimization by iterating the equation self-consistently.

Though the exchange is treated exactly, neglecting the correlation in Hartree-Fock theory is a major shortcoming. This makes the results deviate from experimental ones in many molecular and bulk systems. Although beyond the scope of this thesis, methods for adding the correlation into the HF multi-electron wavefunction exists and they are collectively called post-Hartree-Fock methods[2]. These methods provide more accurate results within the HF framework.

2.2 Density functional theory

An alternative approach to treat the adiabatic version of the many-body hamiltonian in equation 2.2 is DFT[1,3]. It is very popular in solid state physics as it provides a feasible way to study system of the size of 1000 of atoms with acceptable accuracy.

Within DFT functionals of electron density are used to describe the properties of the many-body systems. Although many improvements have been made since the theory was first introduced by Kohn and Sham in 1964, there are still difficulties to properly describe e.g. dispersion, magnetism, strongly correlated systems and band gaps of semiconductors.

DFT is based on the theorems proposed by Hohenberg and Kohn[4]:

1. ground state properties of a many-electron system are uniquely determined by a three dimensional electron density

2. There exists an energy functional $E[n]$ of an electron density that is minimized by the ground state electron density $E[n_{gs}] \leq E[n]$.

The total energy functional uniquely defined by the external potential v_{ext} is written as

$$E_{KS}[n] = T_s[n] + \frac{1}{2}\int d\mathbf{r}d\mathbf{r}^{'}\frac{n(\mathbf{r})n(\mathbf{r}^{'})}{|\mathbf{r}-\mathbf{r}^{'}|} + \int d\mathbf{r}V_{ext}(\mathbf{r})n(\mathbf{r}) + E_{xc}[n], \quad (2.8)$$

where the terms are the kinetic energy of the non-interacting electrons, so-called Hartree energy describing Coulombic electron-electron repulsion, external potential introduced by nuclei and the so-called exchange-correlation energy. All the challenging features of the true many-body problem are hidden in the exchange-correlation term and this term has to be approximated. If the exact form of this term would be available then DFT would be exact.

Within the framework of Kohn and Sham[5] the challenging many-body problem of N-interacting electrons in a static external potential is reduced to a tractable problem of a set of fictitious non-interacting electrons moving in a effective potential

$$-\frac{1}{2}\nabla^2\psi_i(\mathbf{r}) + V_{eff}(\mathbf{r})\psi_i(\mathbf{r}) = \epsilon_i\psi_i(\mathbf{r}), \quad (2.9)$$

where ψ_i are called Kohn-Sham orbitals and reproduce the total electron density

$$n(\mathbf{r}) = \sum_{i=1}^{N}|\psi_i(\mathbf{r})|^2 \quad (2.10)$$

of the original many-body problem. The effective potential

$$V_{eff}(\mathbf{r}) = \int d\mathbf{r}^{'}\frac{n(\mathbf{r}^{'})}{|\mathbf{r}-\mathbf{r}^{'}|} + V_{ext}(\mathbf{r}) + \frac{\delta E_{xc}[n]}{\delta n(\mathbf{r})} \quad (2.11)$$

is the functional derivative of the energy functional and the last term in the previous equation is called the exchange-correlation potential.

Equations 2.9-2.11 are termed the Kohn-Sham equations and together with appropriate approximation to the E_{xc} they provide the basis to solve the equation above in a self-consistent manner.

2.3 Local exchange-correlation functionals

The most common approximations for the exchange-correlation energy are the local density approximation (LDA)[5] and generalized gradient approximation (GGA) that comes with different parameterizations such as PBE[6].

$$E_{xc}^{LDA}[n] = \int d\mathbf{r} n(\mathbf{r}) e_{xc}(n(\mathbf{r})) \tag{2.12}$$

$$E_{xc}^{GGA}[n] = \int d\mathbf{r} n(\mathbf{r}) e_{xc}(n(\mathbf{r})) F_x^{GGA}(\nabla n(\mathbf{r})) \tag{2.13}$$

LDA approximates the XC energy density at given point by the corresponding value of uniform electron gas. This approximation works remarkably well for materials where the electron density variations are very small. GGA's basically enhance this approximation by taking also the gradient of the density at given point into account. This approach works generally better than LDA[7].

To get further insight to these functionals we define the two-electron density

$$\begin{aligned} \rho(\mathbf{r}, \mathbf{r}') &= N(N-1) \sum_{\sigma_2,...,\sigma_N} \int d\mathbf{r_2} ... d\mathbf{r_N} |\Psi(\mathbf{r}, \sigma; \mathbf{r_2}, \sigma_2; ...; \mathbf{r_N}, \sigma_N)|^2 \\ &= n(\mathbf{r}) n(\mathbf{r}^{'}) + n(\mathbf{r}) n_{xc}(\mathbf{r}, \mathbf{r}') \end{aligned} \tag{2.14}$$

where n_{xc} is the exchange-correlation hole. This hole defines the change in the electron density caused by the presence of an electron at r and maps back to the equations 2.12 and 2.13 as

$$E_{xc} = \frac{1}{2} \int d^3r \int d^3r' \frac{n(\mathbf{r}) \overline{n}_{xc}(\mathbf{r}, \mathbf{r}')}{|\mathbf{r} - \mathbf{r}'|}, \tag{2.15}$$

where $\overline{n}_{xc}$ is now the angle-averaged version of the exchange-hole. It is the quality of the approximation for the hole that defines the accuracy of the functional. The LDA and GGA approximations, albeit they are local and based on uniform electron gas, provide a rather good description of the hole for many molecular and bulk materials. This property has made these so-called vanilla type functionals widely used and successful choice to study materials properties.

Despite the success, they have known theoretical shortcomings such as spurious self-interaction where the XC functional does not cancel out electron's interaction with itself present in the Hartree term and the lack of derivative discontinuity[3]. These shortcomings are obvious with i.e. 3d transition metal monoxides like MnO, FeO, CoO and NiO. Vanilla type of functionals underestimate the gap and even give metallic nature for these antiferromagnetic insulators[3].

Also bonding energies are somewhat overestimated, leading to over binding and especially with GGA's the accuracy for structural properties for

heavy elements is rather poor. Furthermore due to the wrong asymptotic decay of exchange potential (exponential instead of 1/r) the description for negative ions fails with vanilla type of functionals[3]. When studying materials where good description for charge localization, magnetic properties and band gaps are essential, it is clear we need to go beyond standard LDA/GGA parameterization.

2.4 Hybrid exchange-correlation functionals

The hybrid approach to generate more accurate functionals was originally introduced by Becke in 1993[8].The approach relies on adiabatic connection[9] and compared to the standard vanilla type functionals, a fraction of the local exchange is replaced by the non-local Fock exchange (exchange operator in equation 2.6 calculated with KS orbitals)

$$E_x^{HF} = -\frac{1}{2}\sum_{k,l}\int d\mathbf{r}_1 d\mathbf{r}_2 \psi_k^*(\mathbf{r}_1)\psi_l^*(\mathbf{r}_2)g(\mathbf{r}_1,\mathbf{r}_2)\psi_k(\mathbf{r}_2)\psi_l(\mathbf{r}_1). \tag{2.16}$$

Including even a small fraction of the non-local operator partly corrects the spurious self-interaction and the lack of derivative discontinuity present in the local functionals[10]. In general these improvements in functionals provide more accurate geometries and energies over vanilla type functionals for many molecular and bulk structures. They also give better description on charge localization, magnetism and provide better values for the band gap[11–20].

The XC energy functional for hybrids is written in the form

$$E_{xc}^{hyb} = aE_x^{local} + (1-a)E_x^{nl} + E_c^{local}, \tag{2.17}$$

where local refers to a (or a mix of) vanilla type functional and nl is the non-local exchange. The mixing parameter a determines how much of the non-local exchange is used in the functional. This is either fitted or theoretically obtained parameter. In this thesis we use hybrid functionals based on PBE0 hybrid functional where the parameter a=0.25 is obtained via perturbation theory[21].

For large scale calculations the previous equation is not feasible due to a huge computational cost. Screened hybrid functionals on the other hand are able to incorporate Fock exchange into bulk materials with significantly lower computational requirements. In addition, screened hybrids functionals lack certain undesirable features experienced with the

full Fock exchange. Without the screening the exchange hole has a tail contribution that is not cancelled out by the local correlation in these functionals. The use of screening reduces the long range tail of the exchange yielding better description for the total exchange-correlation hole. Furthermore for some materials, full exchange overestimates the optical gap. As the screening lowers the amount of exchange, also a better description of the optical gap for these materials is gained. In depth discussion on the properties of the orbital dependent functionals is provided in reference[10].

With screened functionals the Fock integral kernel of 1/r is split into a short-range (SR) and long-range (LR) parts and only the short-range part is included in the functional. In principle this division is arbitrary but the error function below has the benefit of being easily implemented[22]

$$\frac{1}{r_{12}} = \underbrace{\frac{\mathrm{erfc}(\omega r_{12})}{r_{12}}}_{SR} + \underbrace{\frac{\mathrm{erf}(\omega r_{12})}{r_{12}}}_{LR}. \tag{2.18}$$

The parameter ω is again usually obtained via fitting. In the light of our hope for an *ab initio* approach this is not desirable, but nevertheless this approach provides an excellent tool to calculate properties with the accuracy comparable to full hybrid functionals and with a feasible computational cost. The general form of a screened hybrid functional is then given by

$$E_{xc}^{hyb-SR} = aE_x^{local-SR} + (1-a)E_x^{nl-SR} + E_x^{local-LR} + E_c^{local}. \tag{2.19}$$

Here one should also note that also the local functional has been split into SR and LR parts. This is done by introducing comparable screening function into the exchange hole of the local functional[23]. The angle averaged exchange-hole for GGA functional (similarly for LDA) is defined as

$$\overline{n}_x(\mathbf{r}, \mathbf{r}+\mathbf{u}) = \frac{1}{N}\int d^3r \rho^2(\mathbf{r}) J^{GGA}(s(\mathbf{r}), k_F(\mathbf{r})u), \tag{2.20}$$

where $k_F = (3\pi^2\rho)^{1/3}$ is the Fermi wave vector, $s = \frac{|\nabla\rho|}{2k_F\rho}$ the reduced density gradient and J is the function defining the properties of the hole. When screening in form of equation 2.18 is introduced, it transfers to the function J as

$$J^{\omega,GGA,SR}(\rho, s, u) = J^{GGA}(s, u) \times \mathrm{erfc}\left(\frac{\omega u}{k_F}\right). \tag{2.21}$$

The function J onwards relates to the enhancement factor F_X^{GGA} via integral equation

$$F_X^{GGA}(s) = -\frac{8}{9}\int_0^\infty duy J^{GGA}(s, u), \tag{2.22}$$

which then is used to obtain the exchange energy for the given GGA type of functional as

$$E_X^{GGA} = \int d\mathbf{r}\rho(\mathbf{r})\epsilon^{LDA}(\rho(\mathbf{r})) \times F_X^{GGA}(s(\mathbf{r})). \tag{2.23}$$

Here ϵ^{LDA} is the LDA exchange energy density[24].

To get the final expression to the exchange energy $E_x^{SR,GGA}(n, \nabla n)$ of the given functional we need to calculate this integral equation with screened J function explicitly.

In this thesis we have used the PBE[6] GGA functional in publications I and II. All the hybrid functional calculations have been done using the HSE[16] screened hybrid functional

$$E_{xc}^{HSE} = 0.25E_x^{HF-SR} + 0.75E_x^{PBE-SR} + E_x^{PBE-LR} + E_c^{PBE}. \tag{2.24}$$

2.5 Green's functions method for electron transport

To get further insight how a quantum mechanical nanostructure behaves under potential difference we are interested in understanding the transport properties of the material. In general electron transport is a challenging problem as it is a many electron problem in non-equilibrium. The properties of transport in a system are characterized by de Broglie wavelength, the mean free path and the phase relaxation length of electrons.

The de Broglie wavelength is the electron wavelength at the Fermi level. If the size of the system is of the same order or smaller than this length the quantum mechanical properties govern its behavior. In this region Ohm's law is no longer valid and a quantum mechanical approach must be applied.

The mean free path tells us how long a distance an electron travels before losing its original momentum. In collisions, electrons usually lose only part of their momentum and thus the mean free path is longer than the distance travelled between single collisions. Phase-relaxation length gives the average length an electron travels before losing original phase in collisions.

Within this thesis, the studied systems have a phase-relaxation length that is typically large and the sizes of the systems are comparable to the de Broglie wavelength. These scales allow us to simplify the picture by

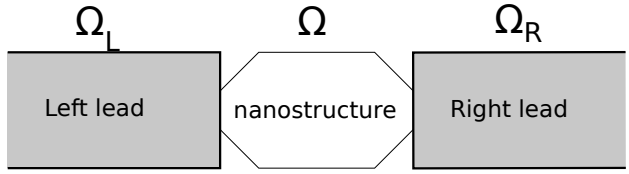

Figure 2.1. General setup for electron transport. Nanostructure (region Ω) is connected to left and right semi-infinite lead $\Omega_{L/R}$. Leads are considered as ideal crystalline structures and nanostructure is the only scattering region.

assuming coherent transport only. This means that the electron phase is conserved.

If we consider a general system as shown in the figure 2.1, the current through the nanostructure can be described by the Landauer formula:

$$I = G_0 \sum_n \int_{\mu_R}^{\mu_L} |t_n(E)|^2 dE, \tag{2.25}$$

where G_0 is the unit conductance and the $|t_n|^2$ gives the probability that incoming electron with energy E is transmitted through the scattering region Ω in conducting mode n. The leads (reservoirs) are assumed to be in thermal equilibrium and perfect thermalization of electrons is also assumed when electrons enter these reservoirs.

Here the studied system are simulated with the setup shown in figure 2.1 using DFT-Green's functions method. The studied nanostructures are connected to semi-infinite leads $\Omega_{L/R}$ with open boundary conditions. This means that electrons can travel from and to the leads without reflections.

Green's functions provide a straightforward way to solve the partial differential equation in the scattering region with open boundary conditions. In addition they allow one to connect the leads with different chemical potential to the system and thus provide a theoretical description where finite-size effects do not play a significant role. The derived solution for the tunneling probabilities and current through the nanostructure is analogous to the Landauer formula (2.25).

The Hamiltonian of the nanostructure is approximated by DFT method described in previous chapters. Here for Kohn-Sham equations single particle Green's functions are used instead of single particle wavefuctions. The starting point is retarded Green's function G^r that is the resolvent operator for equation

$$(\omega - \hat{\mathbf{H}}(\mathbf{r}))G^r(\mathbf{r}, \mathbf{r}'; \omega) = \delta(\mathbf{r}, \mathbf{r}'), \tag{2.26}$$

where ω is the energy and $\hat{\mathbf{H}}$ is obtained using DFT. This equation also gives advanced Green's function G^a as another solution. When G^r is known so-called lesser Green's function $G^<$ can be calculated. When no bias voltage is applied and the system is in equilibrium the $G^<$ is given by

$$G^<(\mathbf{r}, \mathbf{r}^{'}; \omega) = 2 f_{L/R}(\omega) G^r(\mathbf{r}, \mathbf{r}^{'}; \omega). \tag{2.27}$$

Here $f_{L/R}(\omega)$ are the fermi functions of the leads that are equal in the equilibrium.

For finite bias the system must be divided into three regions Ω, Ω_L and Ω_R as show in the figure 2.1. In this case equation 2.26 transforms into

$$(\omega - \hat{\mathbf{H}}(\mathbf{r}) - \Sigma_L^r(\omega) - \Sigma_R^r(\omega)) G^r(\mathbf{r}, \mathbf{r}^{'}; \omega) = \delta(\mathbf{r}, \mathbf{r}^{'}), \tag{2.28}$$

where $\hat{\mathbf{H}}$ is the Hamiltonian of scattering region Ω and $\Sigma_{L/R}^r$ are the so-called self-energies of the leads. These terms describe the electron interaction between Ω and both leads $\Omega_{L/R}$ and couple the solution in scattering region to those on the leads.

Furthermore we define Γ-functions as

$$i\Gamma_{L/R} = 2iIm(\Sigma_{L/R}^r). \tag{2.29}$$

Now $G^<$ for system with finite bias is given by

$$\begin{aligned} G^<(\mathbf{r}, \mathbf{r}^{'}; \omega) = \\ &- i f_R(\omega) \int_{\partial\Omega_R} \int_{\partial\Omega_R} G^r(\mathbf{r}, \mathbf{r_R}; \omega) \Gamma_R(\mathbf{r_R}, \mathbf{r_R^{'}}; \omega) G^a(\mathbf{r_R^{'}}, \mathbf{r}^{'}; \omega) d\mathbf{r}_R d\mathbf{r}_R^{'} \\ &- i f_L(\omega) \int_{\partial\Omega_L} \int_{\partial\Omega_L} G^r(\mathbf{r}, \mathbf{r_L}; \omega) \Gamma_L(\mathbf{r_L}, \mathbf{r_L^{'}}; \omega) G^a(\mathbf{r_L^{'}}, \mathbf{r}^{'}; \omega) d\mathbf{r}_L d\mathbf{r}_L^{'}, \end{aligned} \tag{2.30}$$

where the bias defines the difference between f_L and f_R. When $G^<$ is known, the electron density of the system is given by equation

$$\rho(\mathbf{r}) = -\frac{1}{2\pi} \int_{-\infty}^{\infty} Im[G^<(\mathbf{r}, \mathbf{r}; \omega)] d\omega. \tag{2.31}$$

The solution for equation 2.28 is then obtained in a self-consistent manner by starting from initial guess and iterating until the convergence of the density is below the desired threshold.

When the final solution is obtained we can calculate the current through the nanostructure. For this we calculate the electron tunneling probability between the leads as

$$\begin{aligned} T(\omega) = \int_{\partial\Omega_L} \int_{\partial\Omega_L} \int_{\partial\Omega_R} \int_{\partial\Omega_R} &\Gamma_L(\mathbf{r_L}, \mathbf{r_L^{'}}; \omega) G^r(\mathbf{r_L^{'}}, \mathbf{r_R}; \omega) \\ &\times \Gamma_R(\mathbf{r_R}, \mathbf{r_R^{'}}; \omega) G^a(\mathbf{r_R^{'}}, \mathbf{r_L}; \omega) d\mathbf{r}_L d\mathbf{r}_L^{'} d\mathbf{r}_R d\mathbf{r}_R^{'}. \end{aligned} \tag{2.32}$$

The current is then calculated as

$$I = \frac{1}{\pi}\int_{-\infty}^{\infty} T(\omega)(f_L(\omega) - f_R(\omega))d\omega. \tag{2.33}$$

2.6 Basis sets

In the DFT simulations in addition to the choice of exchange correlation functional, the basis set also contributes significantly to the accuracy. The popular choices in solid state physics are plane waves or atom centered basis sets. Plane waves offer a rigorous way of increasing the accuracy and thus achieving convergence. Atomic centered orbitals on the other hand require less basis functions, making the calculations faster. Also they provide a cheap way to model vacuum making them a good option for studying molecules and surfaces. But compared to plane waves, they do not have a systematic way of increasing accuracy and thus more consideration in choosing a proper basis is needed.

In this thesis we are using a linear combination of atomic orbitals[25,26] (LCAO) as the basis set. Here the KS orbitals are expanded into a linear combination of chosen basis functions

$$\Psi_i^{KS} = \sum_{j=1}^{L} c_{ji}\chi_j, \tag{2.34}$$

where the functions χ_j are now atom centered. For a complete basis L should be infinite, but in practice this is finite and for efficiency as small as possible. Thus, it is essential to choose the basis functions carefully to obtain an accurate approximation for the KS orbitals.

The SIESTA methods used in this thesis have adopted a numerical basis set. Here the atom centered functions are given as

$$\chi_{nlm}(\mathbf{r}) = \sum_{i=1}^{N_{zeta}} R_{nl}^i(r)Y_l^m(\phi,\theta). \tag{2.35}$$

The nlm are the quantum numbers of each atomic orbital and $Y_l^m(\phi,\theta)$ is the spherical harmonic function. The radial part is given by numerical function that has a strict cut-off radius r_c at some distance. The minimal basis set (single-ζ, $N_{zeta} = 1$) refers to a basis where only a single radial function per atomic orbital is used. Within SIESTA this first ζ orbital is obtained by a solution to an isolated atom. Higher ζ's are then obtained as solutions to positively charged atoms.

Also polarization orbital may be added where a solution to a higher angular momentum to the corresponding orbital is added to the basis set. Generally double-ζ ($N_{zeta} = 2$) + polarization provides a good compromise between speed and accuracy in SIESTA.

Another atomic center choice for a basis set commonly used are the cartesian gaussian type functions (CGTO)'s. Here the atom centered functions are given by

$$\chi(\mathbf{r}) = \sum_{i=1}^{N} d_i \eta_i^{GTO},$$
$$\eta^{GTO} = N_{norm} x^l y^n z^m e^{\alpha r^2},$$

where the N_{norm} is the normalization factor, xyz are the cartesian coordinates and α is the exponent determining how extended the basis functions are. Unlike with the SIESTA orbitals here the basis functions in principle extend to infinity. In practical calculations they are truncated to achieve a localized and thus computationally efficient basis.

In this thesis we use CGTO's with the exchange integral in hybrid functionals as there are existing analytical quadratures to solve these kind of integrals. These are only used as an auxiliary basis set for the numerical SIESTA orbitals used in the calculations. We are also doing all the calculations with pseudo potentials and thus the basis set formalism is only used with valence orbitals.

One downside in using LCAO is the basis set superposition error (BSSE)[27]. As the atoms move they drag the basis set with them thus changing the basis set. This can lead to artificial contributions to the energy and forces. Sometimes this contribution is significant and we need to use counterpoise correction[27] to remove this artificial factor.

2.7 Pseudopotential approximation

The pseudopotential approximation[28,29] is another common approximation in practical calculations after the exchange-correlation functional and the basis set. In an atom the core electrons are experiencing a strong $-\frac{Z}{r}$ potential. This combined with the orthogonality requirement makes their wavefunctions strongly oscillatory, making them computationally more expensive as denser mesh near the core is required. At the same time

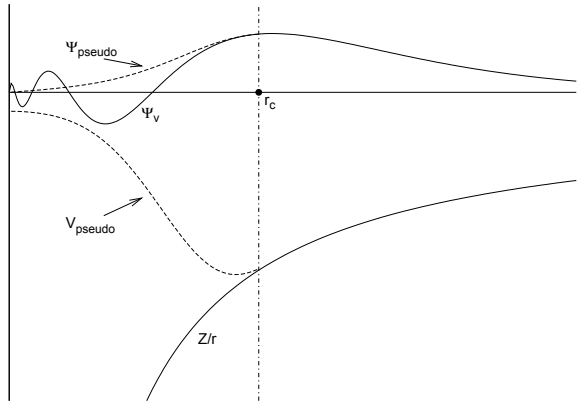

Figure 2.2. Schematic illustration of the pseudopotential (dash-dot line) and all-electron potential (solid) and the corresponding wavefunctions. Pseudopotential and all-electron potential are equal and give the same wavefunctions outside radius r_c.

the core electrons are affected only very little by the surrounding environment. Thus considering these electrons to be fully unaffected by the environment we can construct an effective potential called the pseudopotential to describe their contribution as illustrated in the figure 2.2.

3. Structure optimization and molecular dynamics

To understand how thermal movement of atoms changes the structure or what is the zero-temperature structure of the studied system one needs to calculate forces acting on ions. Within DFT-framework we use adiabatic approximation, as mentioned in the theory chapter, to divide atomic movement from electronic.

After the electronic self-consistent field (SCF) convergence has been reached, forces acting on ions may be calculated using Hellman-Feynman theory[3,30,31]. Here the DFT forces on ion at position R_I are given by

$$\frac{dE}{dR_I} = \frac{\partial E}{\partial R_I} = \frac{\partial < \phi_i|H|\phi_i >}{\partial R_I} =< \phi_i|\frac{\partial H}{\partial R_I}|\phi_i > . \tag{3.1}$$

These forces may then be used to relax the system towards ground-state at zero temperature or perform molecular dynamics at finite temperature. The dynamics for atoms are performed classically. In this section we describe the methods used in this thesis to perform both ionic relaxations and molecular dynamics (MD). For molecular dynamics a classical approach is used.

3.1 Conjugate-gradient method

For the atomic ground-state we usually start from the initial system where there are still significant forces present after the first SCF iteration cycle. These forces are then used to move ions after which new electronic SCF cycle is performed, following a new forces calculation. The task of minimizing the atomic system to the zero-force configuration becomes nontrivial when the system can consist hundreds of atoms.

The minimization techniques used in this thesis can be divided into first and second order methods. An efficient iterative first order method is

the Conjugate-gradient (CG) methods[1] also implemented into the SIESTA code. Here the stationary point of a given function F(x) is a set of points x_i where

$$\left(\frac{\partial F(x)}{\partial x}\right)_{x_i} = g_i = 0. \tag{3.2}$$

The initial optimization direction is taken into the steepest-descent direction. The subsequent search directions are then constructed as a combination of the new negative gradient and the previous search direction. Figure 3.1 illustrates how CG method works.

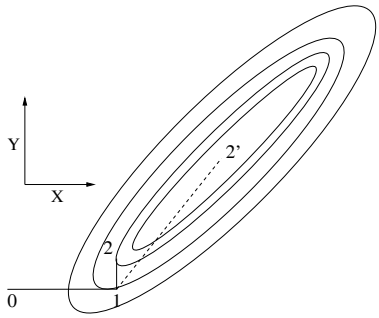

Figure 3.1. Illustration of how CG method works for quadratic function in two dimensions. Ellipses are the contour lines of the minimized function f, solid line present steepest descent method and dashed line CG method. The steepest descent (steps 0,1,2) is quite far from the minimum after two steps while CG method (0,1,2$'$) reaches the minimum with two steps.

3.2 Quasi-Newton method

Another iterative minimization technique used in this thesis is the second order Broyden-Fletcher-Goldfarb-Shanno[32] (BFGS) method. To find a stationary point of the function F(x) in addition to first order derivatives present in CG methods also second order derivatives are used. The matrix of the second order derivatives is called the Hessian matrix

$$\left(\frac{\partial^2 F(x)}{\partial x^2}\right)_{x_i} = H_i. \tag{3.3}$$

In the Newton method, it is assumed that the function can be locally approximated as a quadratic Taylor expansion in the region around the optimum

$$F(x) = F(x_i) + g_i^T(x - x_i) + \frac{1}{2}(x - x_i)^T H_i (x - x_i). \tag{3.4}$$

Requiring the gradient to be zero produces $(x - x_i) = -H^{-1}g$. In quasi-Newton methods the expensive calculation of the Hessian matrix is replaced by gradually building an approximate Hessian from successive gradient vectors. The initial matrix can be simply an identity matrix resembling a steepest-descent approach. The advantage of this method is that it reduces the required steps to reach the stationary point compared to then CG method and in generally outperforms also Newton methods in speed as the expensive Hessian matrix is not calculated.

On the other hand if the system is far from the minimum the BFGS may be rather slow or even take the system to a local minimum instead of the global one. Here CG method should be preferred as it tends to work reliably even far from the global minimum. One may also combine these two approaches by starting with CG method and when closer to the minimum, turn on the second order method.

3.3 Nose Hover thermostat

In experimental situations the temperature is usually kept constant and thus it is desirable to be able to perform MD simulations at constant temperature. One approach is to introduce an extra force acting on the particle with the purpose of keeping the temperature constant. In the Nose-Hoover thermostat[1], coupling to a heat reservoir is done in the form of friction proportional to the particle velocities. The advantage of a Nose-Hoover thermostat is that the time average value of temperature is equal to a prescribed value.

The equations of motions in this approach are given by

$$\frac{d\mathbf{r}_i}{dt} = \frac{\mathbf{p}_i}{m}; \quad \frac{d\mathbf{p}_i}{dt} = \mathbf{F}_i - \zeta \mathbf{p}_i; \tag{3.5}$$

$$\frac{d\zeta}{dt} = (\sum_{i=1}^{N} \frac{p_i^2}{m_i} - 3Nk_BT)/Q, \tag{3.6}$$

where p_i and r_i are the momentum and position of an particle. The magnitude of the Q determines the coupling between the reservoir and the real system. The Q parameter has to be chosen with care as with too small a parameter, the phase space will not be canonical (constant NVT). And with too large a parameter, the heat transfer will not be sufficient.

In the light of this thesis we use finite temperature MD as a way to perform simulated annealing that is an approach to find a good approxi-

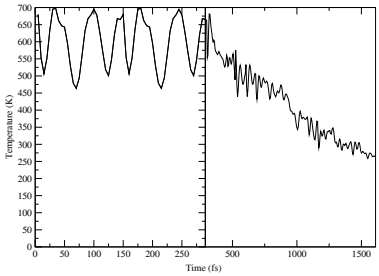

Figure 3.2. Illustration how first Nose-Hoover thermostat is used for MD. The temperature oscillates around the target temperature of 600K. The minimum energy configuration is then approached by slowly annealing the temperature down.

mation to the global minimum of a given function in a large search space. The task of finding equilibrium geometry is rather challenging, especially if one has no pre-knowledge of the final structure. For the studied hafnia interfaces this has been the case. In practice this can be achieved by allowing system to fluctuate at a given high temperature and then slowly cool it down to zero temperature.

3.4 Relaxations in a plane

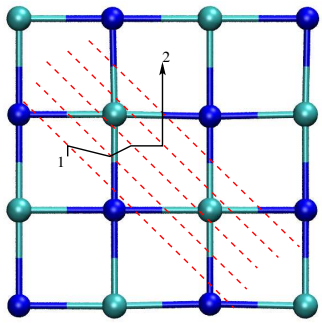

Figure 3.3. Illustration of how the relaxation in a plane algorithm works. We define a normal (110) for the plane and divide our path into plane segments (red dashed lines). The planes are now perpendicular to the image. Now the constrained relaxation in each plane is performed and finally the diffusion path is obtained (black solid line).

For the paper III we implemented constrained relaxation algorithm into the SIESTA code. This allowed us to probe the diffusion path and most

importantly diffusion barrier of an atom on the surface. In practice all paths were calculated at least to (100) and (110) directions. Without any constraints the atom would have relaxed to the closest energy minima. The method is shows in the Figure 3.3.

4. Implementing hybrid functionals

The biggest work in this thesis has been the implementation of the Fock exchange as in equation 2.6 within a DFT framework into the SIESTA code. Furthermore, a screened version of Fock exchange has been included for building screened functionals such as HSE.

For the HSE functional, also a screened version of local PBE exchange has been implemented. These incredients allow a large variety of functionals to be constructed, though we keep the discussion focused on HSE.

In this section an overview of the used algorithms and approaches are presented.

4.1 SIESTA code

SIESTA [25,33] is a real space linear combination of atomic orbitals basis code, implementing the density functional theory (DFT) within the generalized gradient approximation. Core electrons are represented by norm-conserving pseudopotentials using standard Troullier-Martins parameterization. It uses numerical orbitals with a high flexibility wrt. cut-off radii, number of ζ's and number of polarization orbitals used in the calculations. Most of the calculations are done numerically on a real-space grid.

In SIESTA usually only small number of basis functions per atom are required and these orbital are rather localized around the nuclei. Thus SIESTA is relatively fast and makes calculations of hundreds of atoms feasible within a reasonable accuracy. Localized orbitals furthermore make the computational task to scale linearly with respect to system size or number of atoms. Also with localized basis set the user does not pay any

penalty for vacuum in the system making SIESTA a good choice for calculating e.g. surfaces.

4.2 Screened PBE exchange

To obtain the GGA exchange in general we need to have an algorithm for enhancement factor F_X. In the simplest form the general PBE enhancement factor F_X can be written as

$$F_X(s) = 1 + \kappa - \kappa/(1 + \mu s^2/\kappa), \tag{4.1}$$

where κ and μ are parameters of PBE exchange hole [6]. This form has already been implemented into the SIESTA code and has been readily available.

HSE functional needs PBE exchange to be separated into short range and long range parts as shown in equation 2.17. For this, one needs to use the integral formalism shown in equation 2.21. For PBE, J in this is given as [23]

$$\begin{aligned} J^{GGA}(s,y) =& [-\frac{\mathcal{A}}{y^2}\frac{1}{1+(4/9)\mathcal{A}y^2} \\ &+ (\frac{\mathcal{A}}{y^2} + \mathcal{B} + \mathcal{C}[1 + s^2\mathcal{F}(s)]y^2 \\ &+ \mathcal{E}[1 + s^2\mathcal{G}(s)y^4)exp(-\mathcal{D}y^2)] \\ &\times exp(-s^2\mathcal{H}(s)y^2), \end{aligned} \tag{4.2}$$

where $\mathcal{A}$-$\mathcal{H}$ are parameters or parameterized functions of PBE exchange hole. The enhancement factor F_X^{PBE} is then obtained as an integral from equation 2.22 and the integral has an analytical solution [23].

Similar expression can be used for short range (SR) part of F_X with small approximations since for $erfc(x)$ there is no closed form solution. The used approach is to approximate the complementary error function and a product of polynomial and exponent function[34]

$$erfc(x) \approx P_8(x)exp(-bx^2), \tag{4.3}$$

where $P_8(x)$ is 8th order polynomial. In [35] this has been shown to provide very good accuracy for given functional. With this approximation the problem reduced to similar solution as with J^{GGA}.

This algorithm has already been presented in [35] and has been implemented at least to Gaussian and VASP codes. Within this work the algo-

rithm for screened PBE exchange has been rewritten and adopted to the SIESTA code.

4.3 Algorithms for Fock exchange

4.3.1 Rys quadrature

For evaluating the two electron integrals the most efficient and practical way we found was to use analytical expression formulate by Lindh, Ryu and Liu known as the RYS quadrature [36]. Here cartesian Gaussians functions are used to evaluate these integrals.

With SIESTA orbitals we first fit these into an auxiliary basis set of CGTO's. For spherical harmonic part this can be done exactly but the radial component needs to be fitted. Proper amount of gaussians is needed to minimize the mismatch error and SIESTA orbitals are then expressed as

$$\chi_i^{lm}(\mathbf{r}) = \sum_\mu c_{\mu i}\phi_{\mathbf{a}\mu}(\mathbf{r}), \tag{4.4}$$

where the quantum numbers lm are expressed with cartesian exponents **a**=(a_x, a_y, a_z) of the CGTO.

The primitive electron repulsion integral (ERI) of four unnormalized GTO's is a six dimensional integral

$$[\mathbf{a}_\mu \mathbf{b}_\nu|\mathbf{c}_\kappa \mathbf{d}_\lambda] = \int d\mathbf{r}_1 \int d\mathbf{r}_2 \phi_{\mathbf{a}\mu}(\mathbf{r}_1)\phi_{\mathbf{b}\nu}(\mathbf{r}_1)\frac{1}{\mathbf{r}_{12}}\phi_{\mathbf{c}\kappa}(\mathbf{r}_2)\phi_{\mathbf{d}\lambda}(\mathbf{r}_2), \tag{4.5}$$

that needs to be solved. Using the transfer equation[36]

$$(\mathbf{a}(\mathbf{b}+\mathbf{1}_\lambda| = ((\mathbf{a}+\mathbf{1}_\lambda)\mathbf{b}| + (\mathbf{A}_\lambda - \mathbf{B}_\lambda)(\mathbf{ab}|$$
$$\lambda = \text{ x,y,z, and } \mathbf{1}_\lambda = (\delta_{x\lambda}, \delta_{y\lambda}, \delta_{z\lambda}),$$

we can reshape the problem and solve the batches of $[\mathbf{e}0|\mathbf{f}0]$ (where $\mathbf{e} = max(\mathbf{a}, \mathbf{b}, \mathbf{a}+\mathbf{b})$ and $\mathbf{f} = max(\mathbf{c}, \mathbf{d}, \mathbf{c}+\mathbf{d})$) instead of the batch $[\mathbf{ab}|\mathbf{cd}]$. Furthermore using the Laplace transform for 1/r

$$\frac{1}{|\mathbf{r}_1 - \mathbf{r}_2|} = 2\pi^{-1/2}\int_0^\infty du\, exp[-u^2(\mathbf{r}_1 - \mathbf{r}_2)^2] \tag{4.6}$$

and write the products of two gaussians as a new gaussian

$$exp[-\alpha(\mathbf{r}-\mathbf{A})^2] \times exp[-\beta(\mathbf{r}-\mathbf{B})^2] = \kappa_{AB}\, exp[-\zeta(\mathbf{r}-\mathbf{P})^2] \tag{4.7}$$

the the six dimensional integral $[\mathbf{e}0|\mathbf{f}0]$ can be written into a form

$$[\mathbf{e}0|\mathbf{f}0] = \int_0^1 dt P_n(t) exp[-t^2\rho(\mathbf{P}-\mathbf{Q})^2]. \tag{4.8}$$

Here the polynomial $P_n(t)$ is called the RYS polynomial where n is determined by the sum of angular momentums of CGTO's involved. It has analytical expressions and in practice the zeroth order term is evaluated directly and the higher order terms are obtained via recursion. The integrand is finally evaluated exactly by an n-point quadrature as

$$[\mathbf{e}0|\mathbf{f}0] = \sum_{\alpha=1}^{n_{RYS}} P_n(t_\alpha) W_\alpha. \tag{4.9}$$

Finally we reuse the transfer equation to build the expression for primitive ERI's and further use those to get the final expression for an exchange integral over SIESTA orbitals.

4.3.2 Efficient screening

In practical calculations the number of integrals is enormous and this can be a limiting factor, especially for bulk materials. Still only a minor portion of these integrals give a significant contribution and thus efficient pre-screening of integrals has be performed making calculations feasible. The pre-screening neglects integrals yielding a contribution smaller than user defined parameter states. Choosing a proper parameter is thus essential for doing still accurate calculations, but without extra computational work.

The Schwarz inequality[37] gives an upper bound for the integrals with respect to distance of orbital pairs

$$|(\mu\nu|\lambda\sigma)|^2 \leq |(\mu\nu|\mu\nu)||(\lambda\sigma|\lambda\sigma)|, \tag{4.10}$$

where $\mu, \nu, \lambda, \sigma$ represent the orbital indices and the whole expression in parenthesis is just a convenient way to write the exchange integral in shorter notation. This expression is valid for 1/r, SR and LR kernels.

For taking the distance of the two pairs into account, we use the multipole method. For an SR kernel, one way of writing this is

$$(\mu\nu|\lambda\sigma)_{SR} \approx \sum_{l=0}^{L} \sum_{j=0}^{L'} q_l^{\mu\nu}(\mathbf{P}) q_j^{\lambda\sigma}(\mathbf{Q}) \frac{\tilde{C}_{l+j}(\mathbf{R_{PQ}})}{\mathbf{R}_{PQ}^{(l+j)}}. \tag{4.11}$$

Here q are multipole terms, $\tilde{C}$ the multipole coefficients and $\mathbf{R}_{PQ}$ distance between centers of charge distributions P and Q. As the screening is especially important for periodic systems where the usage of SR kernel is well established we write here the expression only for SR kernel. In the code, a similar expression is applicable for both SR and 1/r kernels.

These two methods defined above already provide an excellent screening of unimportant integrals. Furthermore this screening can be enhanced by taking the density matrix elements into account. For semiconducting and insulating systems the density matrix has been show to decay exponentially as

$$\lim_{|\mathbf{r}_1-\mathbf{r}_2|\to\infty} \rho(\mathbf{r}_1,\mathbf{r}_2) exp(-\sqrt{E_{gap}}|\mathbf{r}_1-\mathbf{r}_2|), \tag{4.12}$$

where E_{gap} the energy difference between the highest occupied and lowert unoccupied band or molecular orbital. Multiplying the estimates given by the two previous methods by the corresponding density matrix elements provide yet more accurate estimates for the integrals and hence better screening of elements.

4.4 Parallelization

As nowadays the clusters and supercomputers are more available, the emphasis in the implementation has been in parallel efficiency. We have established the parallelization scheme over the orbital pairs in the calculations allowing linear scaling calculations of the exchange calculation even for a modest size system and over huge amount of CPU's. The code has been designed to be parallel in number of CPU's, memory and system size, easily allowing a hybrid treatment within SIESTA for thousands of atoms.

Scaling properties of a bulk CaF_2 plus interstial with 97 and 291 atoms in Fig. 4.1 show that the SR-HFX solver scales nearly ideally with respect to number of CPU's.

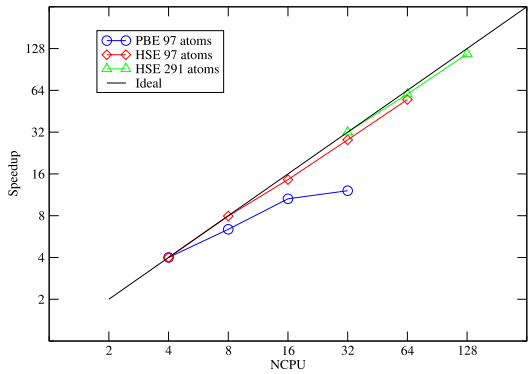

Figure 4.1. Scaling properties of SR-HF solver versus PBE solver. The test system is bulk CaF_2 with 97 and with 291 atoms. Here SIESTA version 2.0.2 is used where PBE scaling is rather poor. This will be improved in future SIESTA releases.

5. Results

5.1 Si-HfO_2 interfaces

Hafnium oxide (HfO_2 or hafnia) still is the leading candidate material to fully or partly replace SiO_2 in metal-oxide-semiconductor field-effect transistors (MOSFETs). Hafnia has a higher dielectric constant which would allow thicker layers to be used to reduce losses due to tunneling compared to silica. Furthermore this would allow the miniaturization to continue beyond the limits set by SiO_2. Though it seems an ideal choice there are many challenges in using hafnia considering the intrinsic properties and the integration into the fabrication process[38–44].

In effort to understand the properties of Si-HfO_2 interfaces and the role of defects we used simulated annealing to construct structures of nonstoichiometric and stoichiometric interfaces with and without saturation with oxygen. Oxygen vacancies were then generated for stoichiometric structures by removing individual oxygens at different sites, after which the structure was again relaxed.

As the system is large and long MD runs were required, the choice of localized basis was a practical one for performing the simulations. All simulations here are done using the SIESTA code using norm-conserving Troullier-Martins pseudopotentials[45] and the GGA functional with Perdew, Burke and Ernzerhof parameterization. We use DZP level basis set, $2 \times 2 \times 1$ kgrid and mesh corresponding to energy cut-off of 150 Ry.

Building of the interface structure was done layer by layer. Initially there were four layers of silicon with bottom dangling bonds terminated by hydrogen atoms. The top dangling bonds were oxygen terminated and

on top of this structure HfO_2 was added in cycles. First one layer is deposited and the system is heated to 600K with Nose thermostat with 5fs steps and then annealed back to zero K. Then relaxed again and the whole deposition cycle is again repeated. The structure creation is most comparable to pulsed laser deposition[46,47] and remote plasma oxidation[48–50]. Finally obtained structures are shows in Fig 5.1 and corresponding electronic structure added with defects are presented in Fig 5.2.

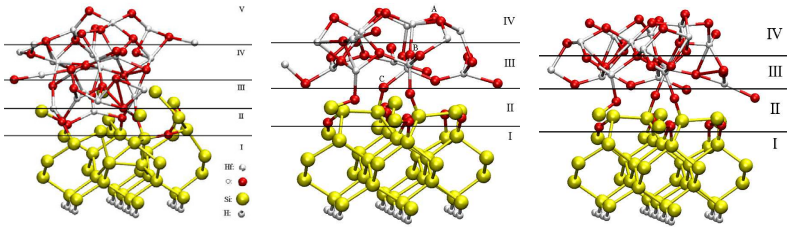

(a) (b) (c)

Figure 5.1. Relaxed structures obtained with simulated annealing for (a) nonstoichiometric Si-HfO_2 interface, (b) stoichiometric Si-HfO_2 interface and (c) stoichiometric Si-HfO_2 interface after addition of saturating oxygen layer.

Our results indicate that direct deposition of HfO_2 on top of silicon yield the creation of undesirable Si-Hf bonds with metallic character. Especially for undercoordinated Hf or with oxygen vacancies this metallic character is clearly observed in both projected density of states and from the electron transport calculations. The main reason is either Hf or oxygen diffusion to the silicon layer and this diffusion has to be prevented in production.

In the light of the methods we know that vanilla type functionals in general underestimate the gap[3,51,52]. The incorrect gap also role when determining whether the defect levels are pinned to conduction band or to the valence band. Thus better methods would provide further insight to the system. It could move the defect levels changing the localization of electrons in the defect or slightly change the geometry also affecting the gap and the stability of defects.

5.2 Adatom diffusion on alkali halide surfaces

The study of metallic nanoclusters has grown in recent years as they relate to real industrial catalysis systems. Although theoretical models are

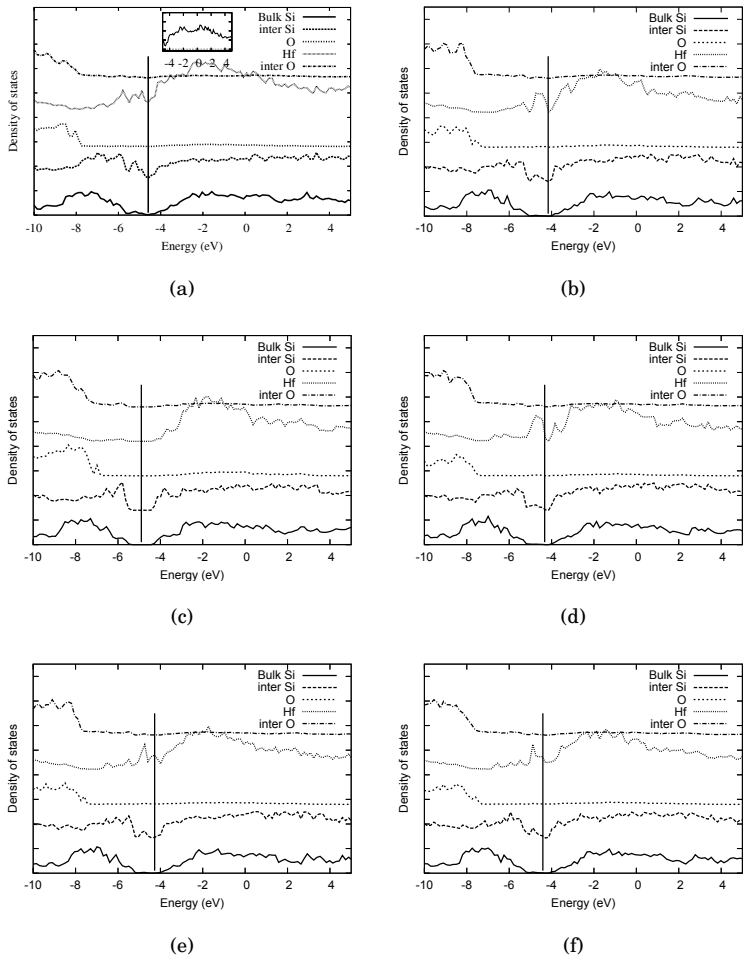

Figure 5.2. Projected density of states for the (a) nonstoichiometric Si-HfO_2, (b) stoichiometric Si-HfO_2 and (c) fully saturated Si-HfO_2. And Projected density of states for HfO_2 with an oxygen vacancy at positions (d) A, (e) B and (f) C in Fig. 5.1. Bulk Si corresponds to silicon atoms in region I of Fig. 5.1, and inter-Si to silicon atoms in regions II and III. The vertical line marks the Fermi energy at the highest occupied molecular orbital.

far from novel devices, they can provide vital insight to the underlying physical processes governing catalysis. Adsorption, growth and formation of these nanoclusters are such important phenomena. In addition charge transfer between the surface and adsorbed atoms influence the nanocluster reactivity and thus is another interesting topic for understanding catalysis.

In paper II we use DFT to study adatom diffusion of Au, Ag and Pd on NaCl(001), KCl(001) and KBr(001) surfaces. We focus on the effects

on charging as scanning probe microscopy (SPM) and scanning tunneling microscopy (STM) have the ability to identify and even change the charge state of individual atoms[53–56] on thin films. For the bulk insulating surfaces considered here similar approaches for individual atoms[57–59] are possible with STM and noncontact atomic force microscopy[60–63] (NC-AFM). Understanding the absorption strength, spin, diffusion barriers and how charging effects these properties and charge stability is crucial in understanding and designing experiments on these benchmark systems.

We use SIESTA code with PBE functional and optimized basis set with several ζ's optimized for each species. Our surface is represented by 2×2 conventional unit-cell slab model and properties were converged wrt. k-points ($1 \times 2 \times 2$) and the mesh (corresponding to energy cut-off of 175 Ry). For absorption energies and sites we have used BSSE correction.

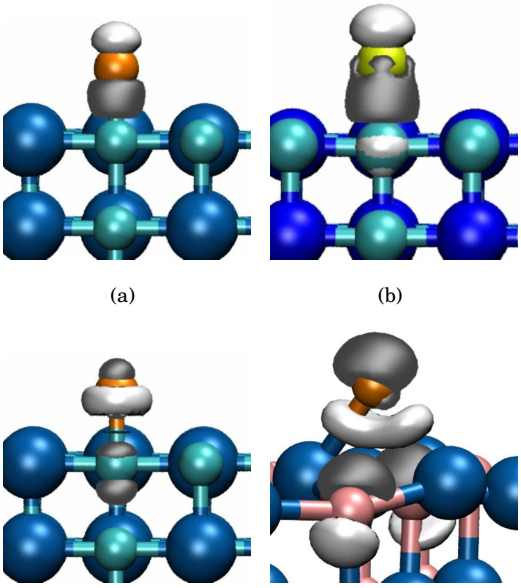

Figure 5.3. Illustration of a few calculated induced charge-density isosurfaces. (a) Ag spin up on KCl, (b) Au spin up on NaCl, (c) Ag spin down on KCl and (d) Ag^- spin up on KBr. Accumulated charge is plotted as a light gray and depleted charge in dark gray isosurface.

Our calculations show that at room temperatures only neutral Pd on NaCl and KCl are valuable candidates for manipulation. With other systems, as shown in the figure 5.4, we see rapid diffusion to more strongly bound sites taking place. For lower temperatures, studying the multiple charge states of silver becomes possible. Different charge states are illus-

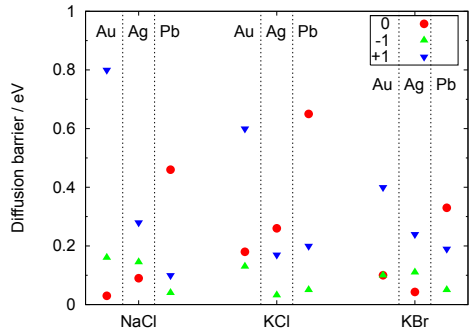

Figure 5.4. Diffusion barrier for Au, Ag and Pb adatoms on NaCl, KCl and KBr substrates. Three charge states (neutral, $\pm$e) are considered.

trated in the figure 5.3. Ag shows charge multistability on NaCl though it is generally weakly bound to the surface and highly mobile regardless of the charge state. For Pd, the neutral charge state is the only stable one and for gold, Au^- is the most stable state across all the surfaces considered.

Again taking the look from the method point of view we know that vanilla type functionals have shortcoming with charge localization. They can e.g. predict unphysical fractional occupations [56]. As the charging and charge stability plays significant role the need for better method is well established.

5.3 Hybrid calculations of semiconducting materials

As stated with previous results the vanilla type of functionals do not always provide accurate enough descriptions, especially for semiconducting and insulating materials. In paper IV we provide hybrid functional implementation of DFT within the SIESTA code. Both the theoretical approach of HSE functional and the implementation is validated by calculating properties of five different bulk materials. These results were compared against PBE and PBESol functionals. Furthermore we have repeated PBE calculation using the VASP code with plane waves and projector augmented wave method to treat the valence and core states, respectively.

Studied systems were CaF_2 , CeO_2 , $NaCl$, TiO_2 (rutile and anatase phases) and HfO_2 (monoclinic, tetragonal and cubic phases). This set of

	Lattice constant (Å)					
System	PBE[a]	PBE[b]	HSE[a]	HSE[b]	PBEsol[a]	Exp.
CaF_2	5.60	5.51, 5.50[64]	5.59	5.47	5.56	5.45[65]
CeO_2	5.43	5.46, 5.43[66]	5.36	5.40	5.36	5.41[67,68]
NaCl	5.69	5.70	5.67	5.66	5.60	5.63[69]
TiO_2	a=3.90	3.81	3.89	3.78	3.85	3.78[70]
anatase	c=9.78	9.68	9.75	9.57	9.74	9.51[70]
TiO_2	a=4.70	4.64, 4.65[71]	4.69	4.59	4.65	4.59[72]
rutile	c=3.03	2.97, 2.97[71]	3.02	2.96	2.99	2.96[72]
HfO_2 cubic	a=5.14	5.08, 5.07[73]	5.13	5.04	5.15	5.08[74]
HfO_2	a=5.12	5.08, 5.06[73]	5.11	5.04	5.13	5.15[75]
tetragonal	c=5.24	5.24, 5.18[73]	5.21	5.16	5.23	5.29[75]
HfO_2	a=5.16	5.13[73]	5.19		5.13	5.12[76]
monoclinic	b=5.23	5.19[73]	5.28		5.30	5.17[76]
	c=5.38	5.31[73]	5.33		5.27	5.30[76]
	β=98.8^o	98.8^o[73]	98.8^o		98.5^o	99.2^o[76]
	Band gap (eV)					
System	PBE[a]	PBE[b]	HSE[a]	HSE[b]	PBEsol[a]	Exp.
CaF_2	6.7	7.4, 8.0[64]	8.8	9.4	6.6	12.1[77]
CeO_2	5.9	6.6	6.2	7.6		6.0[78]
NaCl	5.0	5.0	6.2	6.2	5.0	9.0[79]
TiO_2	1.7	2.4	3.3	3.9		3.2[80]
anatase						
TiO_2	1.5	1.8, 1.7[81]	3.1	3.1	1.5	3.0[82]
rutile						
HfO_2 cubic	3.3	3.8, 3.8 [73]	5.3	5.2		
HfO_2	4.1	4.7, 4.6 [73]	6.0	6.2		
tetragonal						
HfO_2	3.6	4.1[73]	5.1			5.7[83]
monoclinic						

Table 5.1. Lattice constant and band gap values for all calculated systems using SIESTA[a] and VASP[b]. Unreferenced values are calculated in this work. Note that the CeO_2 gap is calculated ignoring the $4f$ states in the gap, as is the usual convention.

systems ranges from narrow to wide gap insulators, and includes a variety of lattice structures and valence character.

With SIESTA we have presented the core electrons by PBE generated norm-conserving pseudopotentials using standard Troullier-Martins parameterization. The basis set for the combined systems was optimized for PBE to provide fast and yet relatively accurate results for ground state properties. The used basis set was double-ζ with polarization for Na($3s^1$), Cl($3p^5$), Hf($6s^2$), O($2p^4$), Ca($4s^2$), Ce($6s^2$), Ti($4s^2$,$3d^2$) and double-ζ for Cl($3s^2$), Hf($5d^2$), O($2s^2$), Ce($5s^2$, $5p^6$, $4f^2$), F($2s^2$,$2p^5$) and single-ζ for Ce($5d^0$). All systems were calculated with a k-point mesh of $7\times7\times7$, a mesh cutoff of 250 Ry and an energy shift of 5 meV. This provided sufficiently high accuracy to converge the lattice structures.

In Table 5.1 a comparison of lattice parameters and band gaps for PBE, PBESol and HSE06 is presented. From a structural point of view HSE06 provides at least as good accuracy as PBE. HSE06 also maintains the hierarchy of phases for TiO_2 and HfO_2 seen for with PBE, with rutile and monoclinic phases predicted as the most stable respectively.

For band gaps the difference for HSE06 becomes more significant as expected. PBE is known to underestimate the gap even by a factor of two as is the case with TiO_2, CaF_2 and NaCl. With HSE, having even a partial amount of exact exchange corrects this for all the systems. For TiO_2, for both phases, the band gap is now in very good agreement with experiment, and for HfO_2 the HSE06 gap is much closer to experiment. But for the wider gap materials, the HSE06 gap experiences a significant underestimation, reflecting the fact that the treatment of exchange is still an approximation [84].

For CeO_2, the difference in band gap between PBE and HSE06 is quite small as PBE already gives a reasonable value, in agreement with previous studies [85]. However, the $4f$-states in the gap, critical in studies of ceria oxidation, are demonstrated to be much closer to the conduction band in HSE06, and this is important when studying defects in ceria and related charge localization [86,87].

In the light of these results we have verified our implementation of a general solver for performing hybrid functional calculations in the SIESTA code. Our results are in good agreement with previous studies, and demonstrate the improvement offered by hybrid functionals in accurate description of electronic structure.

6. Summary

In this thesis we have first studied HfO_2 interfaces. The key findings show that hafnia is an attractive choice to replace silica as a gate insulator but needs further studies. Defects and dangling bonds lead to creation of traps and decrease the gap width. Also a few Si-Hf bonds remained in studied stoichiometries leading to an elevated tunneling probability across the interface. These studies suggest that interface structure must be stabilized to prevent diffusion of hafnium and oxygen. One solution would be to use some chemical precursor to saturate the dangling bonds. But these questions would be topics for future studies.

In the adsorption of metal adatoms on alkali halide surfaces we have studied the role of charge transfer. We have shown how the electronegativity of both adatoms and surface species dominates in the character and strength of the adatom-surface bonds. Though, considering SPM experiments the manipulation becomes extremely challenging. At room temperature for neutral atoms, Pd on NaCl and KCl is the only stable combination, whereas all the other atoms and substrates experience a rapid diffusion. Furthermore, the difference of diffusion barrier between charged states is rather small making the control via charging extremely challenging. Nevertheless, in general this kind of experiment would parallel the study of charge state control already demonstrated on thin films and open the door to the control of adatom mobility via charging.

In contrast to these results we have paid attention to the underlying method. PBE-DFT, a successful and widely used approach, does also have its shortcomings. Especially for previously mentioned systems the theoretical picture for band gap and charge localization does not provide sufficient accuracy. In order to obtain better accuracy we have implemented hybrid functional scheme to the SIESTA code. To assess the method and our implementation we have performed calculation for five different

bulk materials with different electronic properties. Studied systems were CaF_2, CeO_2, TiO_2 as rutile and anatase, NaCl and HfO_2 in monoclinic, tetragonal and cubic phases.

The results for given systems show enhanced accuracy especially for band gap for all the studied systems. Yet it remains clear that even with hybrid approach the theoretical picture is still an approximation. Furthermore we have paid attention to the actual implementation. The chosen algorithm provides hybrid functional results with rather moderate computational cost. For parallel computing the cost is even lower, as our solver scales nearly optimally up to hundreds of cores and possibly even beyond.

The usage of screened hybrid functionals with condensed matter research seems to be growing in general. Methods have found their way into variety of major codes and the approach has matured to be an attractive choice for certain type of systems. The work in this thesis lays the ground for new class of calculations to be performed also with SIESTA method. Applying this method and implementation to the interfaces and surfaces discussed in the first half of this thesis will be something for the future.

Bibliography

[1] J. Thijssen, *Computational Physics* (Campridge Univesity Press, Cambridge, 1999).

[2] F. Jensen, *Introduction to Computational Chemistry 2nd edition* (John Wiley and Sons, Odense, 1999).

[3] C. Fiolhais, *A Primer in Density Functional Theory* (Springer, Berlin, 2003).

[4] P. Hohenberg and W. Kohn, Phys. Rev. **136**, B864 (1964).

[5] W. Kohn and L. J. Sham, Phys. Rev. **140**, A1133 (1965).

[6] J. P. Perdew, K. Burke, and M. Ernzerhof, Phys. Rev. Lett. **77**, 3865 (1996).

[7] V. N. Staroverov, G. E. Scuseria, J. Tao, and J. P. Perdew, Phys. Rev. B **69**, 075102 (2004).

[8] A. Becke, J. Chem. Phys. **98**, 1372 (1993).

[9] J. Harris, Phys. Rev. A **29**, 1648 (1984).

[10] J. Harris, Rev. Mod. Phys. **80**, 3 (2008).

[11] W. K. and. M. C. Holthausen, *A Chemist's Guide to density functional theory* (Wiley, Weinheim, 2001).

[12] J. Heyd, G. E. Scuseria, and M. Ernzerhof, The Journal of Chemical Physics **118**, 8207 (2003).

[13] B. G. Janesko, T. M. Henderson, and G. E. Scuseria, Phys. Chem. Chem. Phys. **11**, 443 (2009).

[14] P. Rivero, I. Moreira, G. E. Scuseria, and F. Illas, Physical Review B **79**, 245129 (2009).

[15] F. Labat, I. Ciofini, and C. Adamo, The Journal of Chemical Physics **131**, 044708+ (2009).

[16] J. Heyd and G. E. Scuseria, The Journal of Chemical Physics **120**, 7274 (2004).

[17] J. Heyd and G. E. Scuseria, The Journal of Chemical Physics **121**, 1187 (2004).

[18] J. Paier, M. Marsman, K. Hummer, G. Kresse, I. C. Gerber, and J. G. Ángyán, The Journal of Chemical Physics **124**, 154709+ (2006).

[19] I. C. Gerber, J. G. Ángyán, M. Marsman, and G. Kresse, The Journal of Chemical Physics **127**, 054101+ (2007).

[20] M. Marsman, J. Paier, A. Stroppa, and G. Kresse, Journal of Physics: Condensed Matter **20**, 064201+ (2008).

[21] M. Ernzerhof and G. E. Scuseria, The Journal of Chemical Physics **110**, 5029 (1999).

[22] J. Toulouse, F. Colonna, and A. Savin, (2004).

[23] M. Ernzerhof and J. P. Perdew, The Journal of Chemical Physics **109**, 3313+ (1998).

[24] A. D. Becke, Phys. Rev. A **38**, 3098 (1988).

[25] J. Junquera, O. Paz, D. Sánchez-Portal, and E. Artacho, Phys. Rev. B **64**, 235111 (2001).

[26] S. García-Gil, A. García, N. Lorente, and P. Ordejón, Physical Review B **79**, 075441 (2009).

[27] S. Simon, J. Bertran, and M. Sodupe, The Journal of Physical Chemistry A **105**, 4359 (2001).

[28] D. R. Hamann, M. Schlüter, and C. Chiang, Phys. Rev. Lett. **43**, 1494 (1979).

[29] N. Troullier and J. L. Martins, Phys. Rev. B **43**, 1993 (1991).

[30] R. P. Feynman, Phys. Rev. **56**, 340 (1939).

[31] J. Hellmann, *Einführung in die Quantenchemie* (Deuticke, Liebzig, 1937).

[32] M. Avriel, *Nonlinear Programming* (Dover Publications, New York, 2003).

[33] J. M. Soler, E. Artacho, J. D. Gale, A. GarcÃa, J. Junquera, P. Ordejón, and D. Sánchez-Portal, J. Phys: Condens. Matter **14**, 2745 (2002).

[34] *Handbook of Mathematical Functions with Formulas, Graphs, and Mathematical Tables*, edited by M. Abramowitz and I. A. Stegun (Dover publications, Washington, 1964).

[35] J. Heyd, Screened Coulomb Hybrid Density Functionals (2004), thesis.

[36] R. Lindh and U. R. and. B. Liu, J. Chem. Phys. **95**, 5889 (1991).

[37] M. Hazewinkel, *Encyclopaedia of Mathematics* (Kluwer, Boston, 1994).

[38] G. D. Wilk, R. M. Wallace, and J. M. Anthony, Journal of Applied Physics **89**, 5243 (2001).

[39] C. D. Young, G. Bersuker, G. A. Brown, P. Lysaght, P. Zeitzoff, R. W. Murto, and H. R. Huff, *in IEEE International Reliability Physics Symposium* (IEEE, New York, 2004).

[40] *High k Gate Dielectrics*, edited by M. Houssa (IOP, London, 2003).

[41] G. Bersuker, Materials Today **7**, 26 (2004).

[42] V. V. Afanas'ev and A. Stesmans, Journal of Applied Physics **95**, 2518 (2004).

[43] A. S. Foster, F. Lopez Gejo, A. L. Shluger, and R. M. Nieminen, Phys. Rev. B **65**, 174117 (2002).

[44] R. Choi, S. C. Song, C. D. Young, G. Bersuker, and B. H. Lee, Applied Physics Letters **87**, 122901 (2005).

[45] N. Troullier and J. L. Martins, Phys. Rev. B **43**, 1993 (1991).

[46] S. J. Wang, P. C. Lim, A. C. H. Huan, C. L. Liu, J. W. Chai, S. Y. Chow, J. S. Pan, Q. Li, and C. K. Ong, Applied Physics Letters **82**, 2047 (2003).

[47] D.-Y. Cho, K.-S. Park, B.-H. Choi, S.-J. Oh, Y. J. Chang, D. H. Kim, T. W. Noh, R. Jung, J.-C. Lee, and S. D. Bu, Applied Physics Letters **86**, 041913 (2005).

[48] B. H. Lee, L. Kang, R. Nieh, W.-J. Qi, and J. C. Lee, Applied Physics Letters **76**, 1926 (2000).

[49] K. Yamamoto, S. Hayashi, M. Niwa, M. Asai, S. Horii, and H. Miya, Applied Physics Letters **83**, 2229 (2003).

[50] H. Takeuchi, D. Ha, and T.-J. King, Journal of Vacuum Science & Technology A: Vacuum, Surfaces, and Films **22**, 1337 (2004).

[51] J. Muscat, A. Wander, and N. Harrison, Chemical Physics Letters **342**, 397 (2001).

[52] J. P. Perdew and M. Levy, Phys. Rev. Lett. **51**, 1884 (1983).

[53] H. Schneider, Helvetica Chimica Acta **65**, 726 (1982).

[54] M. Sterrer, T. Risse, U. M. Pozzoni, L. Giordano, M. Heyde, H.-P. Rust, G. Pacchioni, and H.-J. Freund, Physical Review Letters **98**, 096107 (2007).

[55] J. Repp, G. Meyer, F. E. Olsson, and M. Persson, Science **305**, 493 (2004).

[56] F. E. Olsson, S. Paavilainen, M. Persson, J. Repp, and G. Meyer, Physical Review Letters **98**, 176803 (2007).

[57] N. Oyabu, O. Custance, I. Yi, Y. Sugawara, and S. Morita, Phys. Rev. Lett. **90**, 176102 (2003).

[58] N. Oyabu, Y. Sugimoto, M. Abe, O. Custance, and S. Morita, Nanotechnology **16**, S112 (2005).

[59] Y. Sugimoto, M. Abe, S. Hirayama, N. Oyabu, O. Custance, and S. Morita, Nat Mater **4**, 156 (2005).

[60] R. García and R. Pérez, Surface Science Reports **47**, 197 (2002).

[61] F. J. Giessibl, Rev. Mod. Phys. **75**, 949 (2003).

[62] W. A. Hofer, A. S. Foster, and A. L. Shluger, Rev. Mod. Phys. **75**, 1287 (2003).

[63] A. Foster, *Scanning Probe Microscopy: Atomic Scale Engineering by Forces and Currents* (Springer, Berlin, 2006).

[64] A. Foster, T. Trevethan, and A. Shluger, Physical Review B (2009).

[65] M. Wakaki, K. Kudo, and T. Shibuya, *Physical Properties and Data of Optical Materials (Optical Science and Engineering)* (CRC Press, Boca Raton, 2007).

[66] M. B. Watkins, A. S. Foster, and A. L. Shluger, J. Phys. Chem. C **111**, 15337 (2007).

[67] L. Gerward and J. S. Olsen, Powder Diffr. **8**, 127 (1993).

[68] L. Gerward, J. S. Olsen, L. Petit, G. Vaitheeswaran, V. Kanchana, and A. Svane, J. Alloys Compd. **400**, 56 (2005).

[69] C. Kittel, *Introduction to Solid State Physics* (Wiley, USA, 1995).

[70] M. Horn, C. F. Schwerdtfeger, and E. P. Meagher, Zeitschrift fur Kristallographie **136**, 273 (1972).

[71] G. H. Enevoldsen, H. Pinto, A. S. Foster, M. C. Christensen, A. Kühnle, M. Reichling, W.Hofer, J. V. Lauritsen, and F. Besenbacher, Phys. Rev. B **78**, 045416 (2008).

[72] R. Wyckoff, *Crystal Structures* (Wiley, New York, 1964).

[73] A. S. Foster, F. L. Gejo, A. L. Shluger, and R. M. Nieminen, Phys. Rev. B **65**, 174117 (2002).

[74] J. Wang, H. P. Li, and R. Stevens, J. Mater. Sci. **27**, 5397 (1992).

[75] D. W. Stacy, J. K. Johnstone, and D. R. Wilder, J. Am. Cer. Soc. **55**, 482 (1972).

[76] D. M. Adams, S. Leonard, D. R. Russel, and R. J. Cernik, J. Phys. Chem. Solids **52**, 1181 (1991).

[77] V. E. Borisenko, *Physics, Chemistry and Application of Nanostructures: Reviews and Short Notes to Nanomeeting 2003 Minsk, Belarus 20-23 May 2003* (World Scientific Publishing Company, ADDRESS, 2003).

[78] E. Wuilloud, B. Delley, W. D. Schneider, and Y. Baer, Phys. Rev. Lett. **53**, 202 (1984).

[79] A. K. Cheetham and P. Day, *Solid State Chemistry: Volume 2: Compounds (Oxford Science Publications) (Vol 2)* (Oxford University Press, USA, ADDRESS, 1992).

[80] S. Kowalczyk, Solid State Communications **23**, 161 (1977).

[81] H. P. Pinto, G. H. Enevoldsen, F. Besenbacher, J. V. Lauritsen, and A. S. Foster, Nanotechnology **20**, 264020 (2009).

[82] L. Kavan, M. Grätzel, S. E. Gilbert, C. Klemenz, and H. J. Scheel, J. Am. Chem. Soc. **118**, 6716 (1996).

[83] A. S. Foster, F. Lopez Gejo, A. L. Shluger, and R. M. Nieminen, Phys. Rev. B **65**, 174117 (2002).

[84] M. Marsman, J. Paier, A. Stroppa, and G. Kresse, Journal of Physics: Condensed Matter **20**, 064201 (2008).

[85] J. L. F. Da Silva, M. V. Ganduglia-Pirovano, J. Sauer, and G. Kresse, Physical Review B **75**, (2007).

[86] M. V. Ganduglia-Pirovano, J. L. F. D. Silva, and J. Sauer, Phys. Rev. Lett. **102**, 026101 (2009).

[87] C. Zhang, A. Michaelides, D. A. King, and S. J. Jenkins, Physical Review B **79**, 075433 (2009).

Aalto-DD 219/2013

ISBN 978-952-60-5513-8
ISBN 978-952-60-5514-5 (pdf)
ISSN-L 1799-4934
ISSN 1799-4934
ISSN 1799-4942 (pdf)

Aalto University
School of Science
Department of Applied Physics
www.aalto.fi

BUSINESS +
ECONOMY

ART +
DESIGN +
ARCHITECTURE

SCIENCE +
TECHNOLOGY

CROSSOVER

DOCTORAL
DISSERTATIONS